NOAA Technical Report ERL 367-WPL 45

U.S. DEPARTMENT OF COMMERCE
NATIONAL OCEANIC AND ATMOSPHERIC ADMINISTRATION
Environmental Research Laboratories

Wind and C_n^2 Profiling With Crossed Laser Beams and Spatial Filter Detectors

G.R. OCHS
S.F. CLIFFORD
TING-I WANG

BOULDER, COLO.
MARCH 1976

U.S. DEPARTMENT OF COMMERCE
Elliot L. Richardson, Secretary

NATIONAL OCEANIC AND ATMOSPHERIC ADMINISTRATION
Robert M. White, Administrator
ENVIRONMENTAL RESEARCH LABORATORIES
Wilmot N. Hess, Director

NOAA TECHNICAL REPORT ERL 367-WPL 45

Wind and C_n^2 Profiling With Crossed Laser Beams and Spatial Filter Detectors

G.R. OCHS
S.F. CLIFFORD
TING-I WANG

This report was supported in part by the
U.S. Army Electronics Command,
Atmospheric Sciences Laboratory,
White Sands, N.M. 88002, under W43P65 75-8021
Mr. T.H. Pries was the ASL Scientific Monitor.

Support was also furnished by the
Air Force Weapons Laboratory,
Kirtland Air Force Base, N.M. 87117

BOULDER, COLO.
March 1976

For sale by the Superintendent of Documents, U. S. Government Printing Office, Washington, D. C. 20402

Printed for Atmospheric Sciences Laboratory,
U.S. Army Electronics Command, White Sands Missile Range,
New Mexico 88002, as Research and Development Technical Report
ECOM-76-1. Approved for public release; distribution unlimited.

CONTENTS

WIND AND C_n^2 PROFILING WITH CROSSED LASER BEAMS AND SPATIAL FILTER DETECTORS

G. R. Ochs, S. F. Clifford, and Ting-i Wang

We analyze the potential of crossed laser beams and array receivers to profile wind and C_n^2 along the optical path. The theory of profiling is developed for the cases of multi-detector arrays and two transmitting sources, which may or may not be resolvable. Numerical results based upon the theory are presented, and preliminary experimental results are shown. Finally, we discuss the design of a proposed profiling system, based upon the theory, that will path-resolve wind and C_n^2 into 6 parts over the middle two-thirds of an optical path 0.5 to 2 km long.

1. INTRODUCTION

We have undertaken a theoretical and experimental study of the feasibility of using optical scintillations to measure the profile of the crosswind at various positions along a line-of-sight path. A lower priority task has also been undertaken to investigate the possibility of path-resolving the atmospheric structure constant. The use of artificial light sources of two types are evaluated--one in which different light sources may be identified individually by coding or angular resolution at the receiver, and the other where individual sources are used but not resolved. The general theory of the two concepts is discussed in section 2.1 and 2.2. The research with coded light sources will form the basis for future design and construction of optical wind and C_n^2 profiling systems; the uncoded source work is done to study the possibility of constructing a profiler that uses a natural scene as a light source.

In February, 1975, an additional task was undertaken to deliver a saturation-resistant optical wind measurement system and an operating and service manual, and to publish the theory of operation of the instrument. This phase of the project will be reported separately (Ochs et al., 1976a; Ochs et al., 1976b).

2. THEORY

2.1 C_n^2 and Wind-Weighting Functions Using Resolvable Sources With N-Detector Array

Figure 1 illustrates the geometry of two point transmitters, separated by $\underset{\sim}{\rho}_t$, illuminating two N-element detector arrays, through a turbulence-induced phase screen of amplitude $dn_1(\underset{\sim}{K},s)$ having a two-dimensional spatial wavelength $\underset{\sim}{K}$ and located at position s. The arrays have a wavelength 2a,

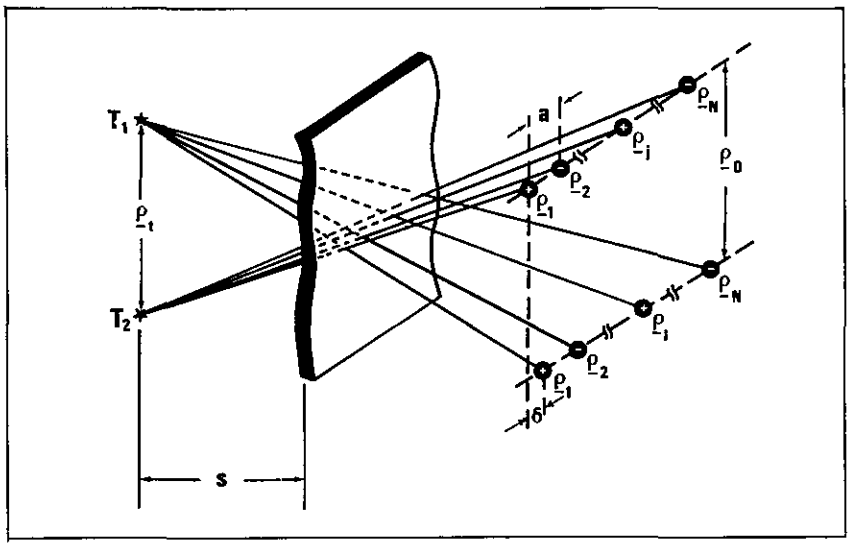

Figure 1. Geometry of the crossed-path spatially filtered detector-array for two resolvable sources.

are separated by a horizontal displacement $\underset{\sim}{\delta}$ and a vertical displacement $\underset{\sim}{\rho}_0$. Following Lee and Harp (1969), we first calculate the total field produced by the lower transmitter as observed by the jth detector in the upper array in the form

$$dE_j = 1-ikdn_1ds \exp\left[\frac{iK^2s(L-s)}{2kL}\right] \cos[\underset{\sim}{K}\cdot\underset{\sim}{\rho}_j s/L-\tfrac{1}{2}\underset{\sim}{K}\cdot\underset{\sim}{\rho}_t(1-s/L)+\underset{\sim}{K}\cdot\underset{\sim}{b}_j] \quad , \tag{1}$$

where $k=2\pi/\lambda$ and λ is the wavelength of the light source, L is the total pathlength and $\underset{\sim}{K}\cdot\underset{\sim}{b}_j$ is an arbitrary phase shift. The amplitude fluctuation observed by the jth detector is given by

$$dP_j=|dE_j|-1 = -kdn_1ds \cos[\underset{\sim}{K}\cdot\underset{\sim}{\rho}_j(s/L)-\tfrac{1}{2}\underset{\sim}{K}\cdot\underset{\sim}{\rho}_t(1-s/L)+\underset{\sim}{K}\cdot\underset{\sim}{b}_j]\sin\left[\frac{K^2s(L-s)}{2kL}\right] \quad . \tag{2}$$

The signal that we will ultimately analyze is the weighted sum of each of the N signals detected by the individual sensors in the array, namely,

$$dP_t=-kdn_1ds \sin\left[\frac{K^2s(L-s)}{2kL}\right]\sum_{j=1}^{N}(-1)^{j-1}\cos[\underset{\sim}{K}\cdot\underset{\sim}{\rho}_j(s/L)-\tfrac{1}{2}\underset{\sim}{K}\cdot\underset{\sim}{\rho}_t(1-s/L)+\underset{\sim}{K}\cdot\underset{\sim}{b}_j] \; . \tag{3}$$

For the upper array in figure 1, we have $2\underset{\sim}{\rho}_j=\underset{\sim}{\rho}_0-\underset{\sim}{a}(N-2j+1)$. In a similar manner, we may write for the response of the lower array

$$dP_t = -kdn_1ds \sin\left[\frac{K^2s(L-s)}{2kL}\right]\sum_{\ell=1}^{N}(-1)^{\ell-1}\cos[\underset{\sim}{K}\cdot\underset{\sim}{\rho}_\ell(s/L)-\tfrac{1}{2}\underset{\sim}{K}\cdot\underset{\sim}{\rho}_t(1-s/L)+\underset{\sim}{K}\cdot\underset{\sim}{c}_\ell] \; . \tag{4}$$

To find the covariance function, we multiply (3) and (4) and take the expected value

$$dC_a = K \int_0^L ds \sin\left[\frac{K s (L-s)}{2kL}\right] \int_0^L ds \sin\left[\frac{K s (L-s)}{2kL}\right]$$
$$<dn_1(\underset{\sim}{K},s_1) \sum_{j=1}^{N} (-1)^j \cos[\underset{\sim}{K}\cdot\underset{\sim}{\rho}_j(s_1/L)-\tfrac{1}{2}\underset{\sim}{K}\cdot\underset{\sim}{\rho}_t(1-s_1/L)+\underset{\sim}{K}\cdot\underset{\sim}{b}_j]dn_1(K,s_2) \qquad (5)$$
$$\sum_{\ell=1}^{N} (-1)^{\ell} \cos[\underset{\sim}{K}\cdot\underset{\sim}{\rho}_\ell(s_2/L+\tfrac{1}{2}\underset{\sim}{K}\cdot\underset{\sim}{\rho}_t(1-s_2/L)+\underset{\sim}{K}\cdot\underset{\sim}{c}_\ell\ ]> ,$$

where the angle brackets indicate an ensemble average. In writing (5), we have allowed a single size of phase screen to be distributed uniformly along the path. Then, by integrating over s_1 and s_2, we have calculated the contribution of all of these to the received signal. Later, we will generalize the result to include a full spectrum of refractive turbulence sizes at each path position. We can calculate the expected value in (5) by first interchanging averaging and summing operators and then by decomposing the sinusoidal phase screen into its two counter-rotating phasor components, that is,

$$<> = \sum_{j=1}^{N} (-1)^j \sum_{\ell=1}^{N} (-1)^{\ell} <[d\psi(\underset{\sim}{K},s_1)e^{i\underset{\sim}{K}\cdot\underset{\sim}{\xi}_1}+d\psi(-\underset{\sim}{K},s_1)e^{-i\underset{\sim}{K}\cdot\underset{\sim}{\xi}_1}]$$
$$[d\psi(\underset{\sim}{K},s_2)e^{i\underset{\sim}{K}\cdot\underset{\sim}{\xi}_2}+d\psi(-\underset{\sim}{K},s_2)e^{-i\underset{\sim}{K}\cdot\underset{\sim}{\xi}_2}]> , \qquad (6)$$

where $d\psi = dn_1 \exp[i\underset{\sim}{K}\cdot\underset{\sim}{b}_j]$, $\underset{\sim}{\xi}_1 = \underset{\sim}{\rho}_j(s_1/L) - \tfrac{1}{2}\underset{\sim}{\rho}_t(1-s_1/L)$ and $\underset{\sim}{\xi}_2 = \underset{\sim}{\rho}_\ell(s_2/L) + \underset{\sim}{\rho}_t(1-s_2/L)$. We now use the following relationships for $d\psi$ given by Lee and Harp (1969), $d\psi(\underset{\sim}{K},s) = d\psi^*(-\underset{\sim}{K},s)$ and

$$<d\psi(\underset{\sim}{K}_1,s_1)d\psi^*(\underset{\sim}{K}_2,s_2)> = \delta(\underset{\sim}{K}_1-\underset{\sim}{K}_2)F_n(\underset{\sim}{K}_1,s_1-s_2)d^2\underset{\sim}{K}\ d^2\underset{\sim}{K}. \qquad (7)$$

In (7), F_n is the two-dimensional spectral density for the refractivity fluctuations. It is related to the three-dimensional refractivity spectrum by means of the relation

$$\Phi_n(K_1,K_2,K_3) = (2\pi)^{-1} \int_{-\infty}^{\infty} F_n(K_2,K_3,s)\cos(K_1 s)ds. \qquad (8)$$

Using the above relations, we can reduce (6) to the form

$$<> = F_n(\underset{\sim}{K},s_1-s_2)\sum_{j=1}^{N}\sum_{\ell=1}^{N}(-1)^j(-1)^{\ell}\cos\left\{\underset{\sim}{K}\cdot[(\underset{\sim}{\rho}_j s_1-\underset{\sim}{\rho}_\ell s_2)/L-\underset{\sim}{\rho}_t(1-\frac{s_1+s_2}{2L})]\right\} . \qquad (9)$$

We now substitute (9) into (5) and, following Tatarskii (1961), we let $2z = s_1+s_2$, $\eta = s_1-s_2$ and make the approximation $K^2/(2k) \ll 1$. The net effect of these assumptions is to set $\eta = 0$ (except in F_n) inside the integral of (5), that is,

$$dC_a = 2k^2 \int_0^L dn F_n(\underset{\sim}{K},n) \int_0^L dz \sin^2\left[\frac{K^2 z(L-z)}{2kL}\right] \sum_{j=1}^{N}\sum_{\ell=1}^{N}(-1)^j(-1)^{\ell} \cos\left\{\underset{\sim}{K}\cdot[(\underset{\sim}{\rho}_j-\underset{\sim}{\rho}_\ell)z/L-\underset{\sim}{\rho}_t(1-z/L)]\right\} . \qquad (10)$$

Because $F_n(\underset{\sim}{K},\eta)$ falls off rapidly (see Tatarskii, 1961 Chapter 7) for $\eta \geq L_0$, where L_0 is the outer scale of refractive-index inhomogeneities, if $L>>L_0$ we can extend the region of integration over η to infinity with negligible error and use (8) to obtain

$$\int_0^\infty d\eta\, F_n(\underset{\sim}{K},\eta)=\pi\Phi_n(0,\underset{\sim}{K}) \tag{11}$$

After substituting (11) into (10) and integrating over a spectrum of turbulence sizes, we obtain

$$C_a=2\pi k^2\int_0^L dz \int d^2\underset{\sim}{K}\, \Phi_n(0,\underset{\sim}{K})\sin^2\left[\frac{K^2z(L-z)}{2kL}\right]\sum_{j=1}^{N}\sum_{\ell=1}^{N}(-1)^j(-1)^\ell \cos\left\{\underset{\sim}{K}\cdot[(\underset{\sim}{\rho}_j-\underset{\sim}{\rho}_\ell)z/L-\underset{\sim}{\rho}_t(1-z/L)]\right\} \tag{12}$$

If we assume isotropic refractive turbulence, that is $\Phi_n(0,\underset{\sim}{K})=\Phi_n(K)$, we may let $d^2\underset{\sim}{K}=KdKd\theta$ and integrate (12) over angles to obtain

$$C_a=4\pi^2k^2\int_0^L dz\int_0^\infty dK K\Phi_n(K)\sin^2\left[\frac{K^2z(L-z)}{2kL}\right]\sum_{j=1}^{N}\sum_{\ell=1}^{N}(-1)^\ell(-1)^j\, J_0[K|(\underset{\sim}{\rho}_j-\underset{\sim}{\rho}_\ell)z/L-\underset{\sim}{\rho}_t(1-z/L)|] \tag{13}$$

To continue, we note the definition of $\underset{\sim}{\rho}_\ell$ and $\underset{\sim}{\rho}_j$ in terms of $\underset{\sim}{a}$, N, $\underset{\sim}{\rho}_0$ and their indices and write

$$\underset{\sim}{\rho}_j - \underset{\sim}{\rho}_\ell = \underset{\sim}{\rho}_0 - \underset{\sim}{\delta} + \underset{\sim}{a}\,(j-\ell). \tag{14}$$

Finally, we compute the magnitude of the vector inside the Bessel function

$$|(\underset{\sim}{\rho}_j-\underset{\sim}{\rho}_\ell)z/L-\underset{\sim}{\rho}_t(1-z/L)| = [(\underset{\sim}{\rho}_j-\underset{\sim}{\rho}_\ell)^2z^2/L^2+\underset{\sim}{\rho}_t^2(1-z/L)^2-2\underset{\sim}{\rho}_t\cdot(\underset{\sim}{\rho}_j-\underset{\sim}{\rho}_\ell)(z/L)(1-z/L)]^{\frac{1}{2}} \tag{15}$$

From figure 1 we know that $\underset{\sim}{\xi} \parallel \underset{\sim}{a}, \underset{\sim}{\rho}_0 \parallel \underset{\sim}{\rho}_t$ and $\underset{\sim}{a}\perp\underset{\sim}{\rho}_t$ so (15) reduces to

$$= \sqrt{[a(j-\ell)-\delta]^2u^2+\beta^2} \tag{16}$$

where $\beta^2=[\rho_0\, z/L-\rho_t(1-z/L)]^2$.

To put (13) in a more useful form, we set $u=z/L$ and note by direct expansion that the double sum may be replaced by

$$\sum_{j=1}^{N}(-1)^j\sum_{\ell=1}^{N}(-1)^\ell[\,] = N\,J_0\left[K\sqrt{\delta^2u^2+\beta^2}\right]+\sum_{m=1}^{N}(-1)^m(N-m)$$
$$\left\{J_0[K\sqrt{(ma-\delta)^2u^2+\beta^2}]+J_0[K\sqrt{(ma+\delta)^2u^2+\beta^2}]\right\}. \tag{17}$$

If we make the usual assumption of a Kolmogorov spectrum of turbulence for Φ_n (Tatarskii, 1961, 1971, namely,

$$\Phi_n(K) = 0.033\, C_n^2\, K^{-11/3};\ L_o^{-1} << K << \ell_o^{-1}\ , \tag{18}$$

where ℓ_0 is the inner and L_0 is the outer scale of refractive turbulence, we obtain the final expression for the covariance function of two spaced-N-element filters,

$$C_a(\delta,\rho_o,\rho_t) = 0.132\pi^2k^2L\int_0^1 du C_n^2(u)\int_o^\infty dK\ K^{-8/3}\ \sin^2\left[\frac{K^2Lu(1-u)}{2k}\right] \tag{19}$$

$$\left\{NJ_o\ [K\sqrt{\delta^2u^2+\beta^2}]+\sum_{m=1}^{N}(-1)^m(N-m)[J_o[K\sqrt{(ma-\delta)^2u^2+\beta^2}]+\ J_o[K\sqrt{(ma+\delta)^2u^2+\beta^2}]]\right\},$$

where $\beta^2=[\rho_0u-\rho_t(1-u)]^2$.

For our C_n^2 profiling experiments, to be discussed in later sections, we measured the covariance with a zero shift, that is, $\delta=0$. In this case, the important consideration to determine path resolution is the C_n^2 weighting function defined by the expression

$$C_a(0,\rho_o,\rho_t) = \int_o^1 du\ C_n^2(u)\ W_1(u,\rho_o,\rho_t) \tag{20}$$

where W_1 is the path weighting function for C_n^2 given by

$$W_1(u,\rho_o,\rho_t) = 0.132\pi^2k^2L\int_o^\infty dK\ K^{-8/3}\ \sin^2\left[\frac{K^2Lu(1-u)}{2k}\right] x \tag{21}$$

$$\left\{NJ_o[K\beta]\ +\ 2\sum_{m=1}^{N}(-1)^m(N-m)\ J_o[K\sqrt{m^2a^2u^2+\beta^2}]\right\}\ .$$

If we let $a \to \infty$, (21) reduces to the result of the two single-detector crossed-path case, which is shown in (12) of our previous paper (Wang et al., 1974).

As part of the effort on the current contract, we investigated wind profiling using the same spatial filter arrays. To analyze this case, we return to the general expression for the covariance function (19). For measuring winds we use the shifted filter expression and insert the time dependence for frozen turbulence drifting across the beam using Taylor's hypothesis (Clifford, 1971); that is, we replace δ in (19) by $\delta-v\tau/u$, where v is the component of the horizontal wind velocity parallel to the N-element arrays. We detect the signal proportional to the wind speed by measuring the slope of the covariance function at zero time-lag, $\tau=0$(Lawrence et al., 1972). Mathematically, this implies that we must differentiate (19) with respect to τ and set $\tau=0$ to obtain the desired expression. The slope at zero time lag is then given by

$$m = \int_0^1 du C_n^2(u) v(u) W_2(u, \rho_0, \delta, \rho_t). \tag{22}$$

(In the experimental work to follow in later sections we set $\delta = a/2$.) After differentiating we obtain W_2 in the form

$$W_2 = 0.066\pi^2 k^2 La u \int_0^\infty dK\, K^{-5/3} \sin^2\left[\frac{K^2 Lu(1-u)}{2k}\right] \left\{ \frac{N J_1(\sqrt{a^2u^2/4+\beta^2})}{\sqrt{a^2u^2/4+\beta^2}} \right.$$

$$\left. + \sum_{m=1}^{N} (-1)^m (N-m) \left[(2m+1) \frac{J_1(\sqrt{(m+1/2)^2 a^2 u^2 + \beta^2})}{\sqrt{(m+1/2)^2 a^2 u^2 + \beta^2}} - (2m-1) \frac{J_1(\sqrt{(m-1/2)^2 a^2 u^2 + \beta^2})}{\sqrt{(m-1/2)^2 a^2 u^2 + \beta^2}} \right] \right\} . \tag{23}$$

Finally, we note in (22) that the wind measurement is modulated by the path distribution of C_n^2. There are several techniques that can be used to eliminate this effect at least to first order by properly normalizing (22). This problem will be discussed in the experimental section to follow.

2.2 Unresolvable Sources with an N-Detector Array

The difference between the resolvable and unresolvable configuration of sources is that, for unresolvable sources, the detector arrays will observe the signal from both transmitters whereas for resolvable sources each detector array receives a signal from one transmitter only. Hence the total field observed by the jth detector in the upper array is

$$dE_j = 1 - i\, k\, dn_1 ds \exp\left[\frac{iK^2 s(L-s)}{2kL}\right] \left\{ \cos\left[\underset{\sim}{K}\cdot\underset{\sim}{\rho}_j (s/L) - \tfrac{1}{2}\underset{\sim}{K}\cdot\underset{\sim}{\rho}_t (1-s/L) + \underset{\sim}{K}\cdot\underset{\sim}{b}_j\right] \right.$$

$$\left. + \cos\left[\underset{\sim}{K}\cdot\underset{\sim}{\rho}_j (s/L) + \tfrac{1}{2}\underset{\sim}{K}\cdot\underset{\sim}{\rho}_t (1-s/L) + \underset{\sim}{K}\cdot\underset{\sim}{b}_j\right] \right\} . \tag{24}$$

Here the first term in the parentheses is from the lower source, while the second term is from the upper source. Closely following the derivation of the resolvable case shown in the last section, we find that the covariance of the amplitude fluctuations of the two N-detector arrays is

$$C_a(\delta, \rho_0, \rho_t) = \int_0^1 du\, C_n^2(u) W_1'(u) \quad , \tag{25}$$

where

$$W_I'(u) = 0.132\pi^2 k^2 L \int_0^\infty dK\, K^{-8/3} \sin^2\left[\frac{K^2 Lu(1-u)}{2k}\right] \Big\{ N\, J_0\left[K\sqrt{\delta^2u^2+\beta^2}\right] + N\, J_0\left[K\sqrt{\delta^2u^2+\beta'^2}\right]$$

$$+ 2N\, J_0\left[K\sqrt{\delta^2u^2+\beta_0^2}\right] + \sum_{m=1}^{N} (-1)^m (N-m) \Big(J_0\left[K\sqrt{(ma-\delta)^2u^2+\beta^2}\right] + J_0\left[K\sqrt{(ma+\delta)^2u^2+\beta^2}\right]$$

$$+ J_0\left[K\sqrt{(ma-\delta)^2u^2+\beta'^2}\right] + J_0\left[K\sqrt{(ma+\delta)^2u^2+\beta'^2}\right] \qquad (26)$$

$$+ 2J_0\left[K\sqrt{(ma-\delta)^2u^2+\beta_0^2}\right] + 2J_0\left[K\sqrt{(ma+\delta)^2u^2+\beta_0^2}\right] \Big) \Big\}$$

where $\beta=\rho_0 u-\rho_t(1-u)$, $\beta'=\rho_0 u+\rho_t(1-u)$, and $\beta_0=\rho_0 u$.

The terms containing β^2 are the contributions to the covariance from the crossed-paths b and c (see figure 2a); hence they agree with the result for the resolvable case (21). The terms involving β'^2 arise from the correlation of paths a and d. The terms containing β_0^2 are contributions from the correlation of paths a and b, and paths c and d. For small ρ_0 and ρ_t (less than a Fresnel zone), the contribution from the crossover location is severely contaminated by the contribution from the other paths. It is not possible to measure the path profile in this case. However, when both ρ_0 and ρ_t are large compared with a Fresnel zone, the contributions

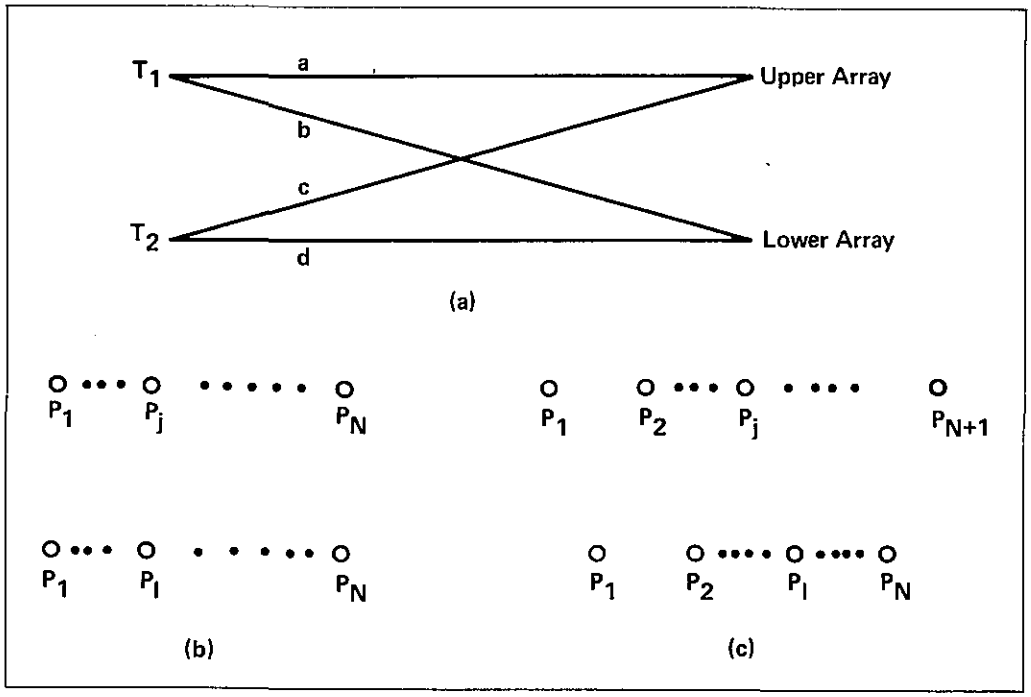

Figure 2. (a) Geometry of the crossed-path technique for two unresolvable sources. (b) Geometry of the detector-array in receiving plane for C_n^2 measurement. (c) Geometry of the detector-array in receiving plane for wind measurement.

from the terms involved, β'^2 and β_0^2, are small compared with the contributions from the terms containing β^2. In this case, the contributions from the crossover location are dominant. For $\delta=0$, we have

$$W_1(u)=0.132\pi^2k^2L\int_0^\infty dK\ K^{-8/3}\sin^2\left[\frac{K^2Lu(1-u)}{2k}\right]\left\{N\ J_0(K\beta)+N\ J_0(K\beta')+2N\ J_0(K\beta_0)\right. \tag{27}$$

$$\left. + 2\sum_{m=1}^{N}(-1)^m(N-m)\left[J_0(K\sqrt{m^2a^2u^2+\beta^2}) + J_0(K\sqrt{m^2a^2u^2+\beta'^2}) + 2\ J_0(K\sqrt{m^2a^2u^2+\beta_0^2})\right]\right\}$$

For wind measurement, we use a different geometry. We use an N-detector array for one receiver, and an (N+1)-detector array for the other receiver such that when $\delta=\frac{1}{2}$, the receivers are symmetric with respect to the center of the array (see figure 2c). Again, closely following the derivation of the results for resolvable sources, we obtain (for $\delta=a/2$)

$$m' = \int_0^1 du\ C_n^2(u)\ v_\perp(u)W_{2\perp}(u,\rho_0,a/2,\rho_t) \quad , \tag{28}$$

where

$$W_{2\perp}=0.066\pi^2k^2Lau\int_0^\infty dK\ K^{-5/3}\sin^2\left[\frac{K^2Lu(1-u)}{2k}\right]\left\{\frac{N\ J_1(\sqrt{a^2u^2/4+\beta^2})}{\sqrt{a^2u^2/4+\beta^2}} + \frac{N\ J_1(\sqrt{a^2u^2/4+\beta'^2})}{\sqrt{a^2u^2/4+\beta'^2}}\right.$$

$$+ \frac{2N\ J_1(\sqrt{a^2u^2/4+\beta_0^2})}{\sqrt{a^2u^2/4+\beta_0^2}} + \sum_{m=1}^{N}(-1)^m\left[(N-m)(2m+1)\left(\frac{J_1(\sqrt{(m+\frac{1}{2})^2a^2u^2+\beta^2})}{\sqrt{(m+\frac{1}{2})^2a^2u^2+\beta^2}} + \frac{J_1(\sqrt{(m+\frac{1}{2})^2a^2u^2+\beta'^2})}{\sqrt{(m+\frac{1}{2})^2a^2u^2+\beta'^2}}\right.\right.$$

$$\left. + \frac{2\ J_1(\sqrt{(m+\frac{1}{2})^2a^2u^2+\beta_0^2})}{\sqrt{(m+\frac{1}{2})^2a^2u^2+\beta_0^2}}\right) - (N-m+1)(2m-1)\left(\frac{J_1(\sqrt{(m-\frac{1}{2})^2a^2u^2+\beta^2})}{\sqrt{(m-\frac{1}{2})^2a^2u^2+\beta^2}} + \frac{J_1(\sqrt{(m-\frac{1}{2})^2a^2u^2+\beta'^2})}{\sqrt{(m-\frac{1}{2})^2a^2u^2+\beta'^2}}\right.$$

$$\left.\left. + \frac{2\ J_1(\sqrt{(m-\frac{1}{2})^2a^2u^2+\beta_0^2})}{\sqrt{(m-\frac{1}{2})^2a^2u^2+\beta_0^2}}\right)\right]\right\} \quad . \tag{29}$$

If we substitute m+1 for m in the second term inside the square parentheses, we have

$$W_{2\perp} = 0.066\pi^2k^2Lau\int_0^\infty dK\ K^{-5/3}\sin^2\left[\frac{K^2Lu(1-u)}{2k}\right]\sum_{m=0}^{N-1}(2N-2m)(-1)^m(2m+1)\left\{\frac{J_1(\sqrt{(m+\frac{1}{2})^2a^2u^2+\beta^2})}{\sqrt{(m+\frac{1}{2})^2a^2u^2+\beta^2}}\right. \tag{30}$$

$$\left. + \frac{J_1(\sqrt{(m+\frac{1}{2})^2a^2u^2+\beta'^2})}{\sqrt{(m+\frac{1}{2})^2a^2u^2+\beta'^2}} + \frac{2\ J_1(\sqrt{(m+\frac{1}{2})^2a^2u^2+\beta_0^2})}{\sqrt{(m+\frac{1}{2})^2a^2u^2+\beta_0^2}}\right\} \quad .$$

In (28) and (29), the notation $\perp$ denotes the vector component perpendicular to the line joining the center of the two sources. It can be shown that the contribution from the wind parallel to the line joining the center of the two sources is completely cancelled out because of the geometry of the spatial arrays (see figure 2c). Hence this setup will detect only the wind component perpendicular to the line joining the two sources. As in the case for C_n^2 measurement, if ρ_t and ρ_0 are small, the wind measurement is contaminated by the contributions outside the crossover region. However, if both ρ_t and ρ_0 are large compared with a Fresnel zone, the path weighting function is sharply peaked at the crossover position.

2.3 Discussion of Numerical Results

The integral over K in (21) and (23) is carried out numerically. The results of the path-weighting functions for C_n^2 measurements are shown in figure 3, where $\rho_0=\rho_t=4\sqrt{\lambda L}$. By varying the spatial wavelength d of the receiver from $0.2\sqrt{\lambda L}$ to $2\sqrt{\lambda L}$, we obtain the path-weighting functions in figure 3. The dash-line curve (d=2) is similar to the results obtained

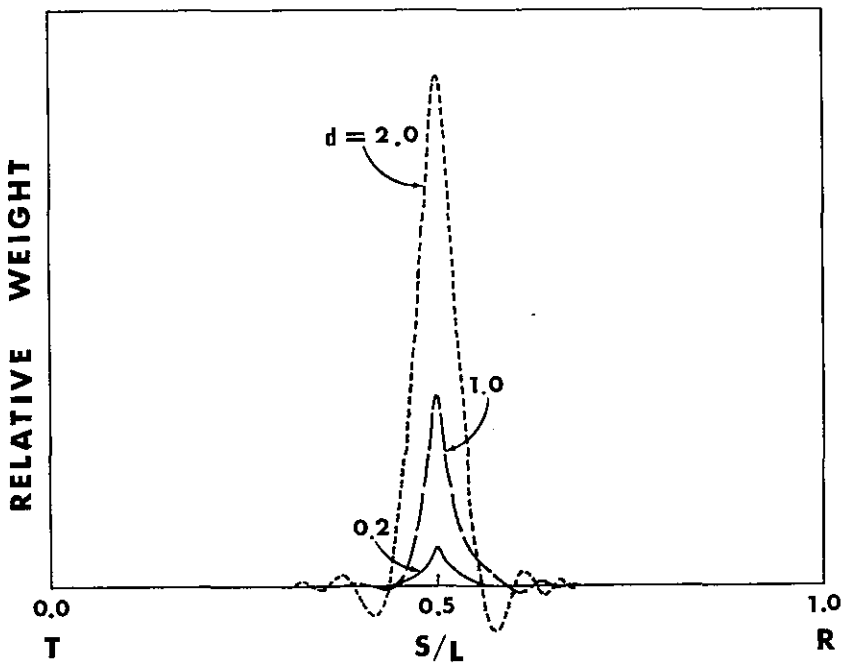

Figure 3. Path-weighting functions for crossed-path spatially filtered detector-array technique for C_n^2 measurements, where $\rho_0=\rho_t=4(\lambda L)^{\frac{1}{2}}$, N=4 and d is the spatial wavelength.

without using a spatially filtered receiver. For smaller spatial wavelength, the weighting functions are similar. In figure 3, we set the number of detectors equal to 4 (i.e., two wavelengths). By increasing the number of detectors from N=4 to 16, we obtain the results plotted in figure 4 with d=0.2. The shapes of the weighting functions change very little.

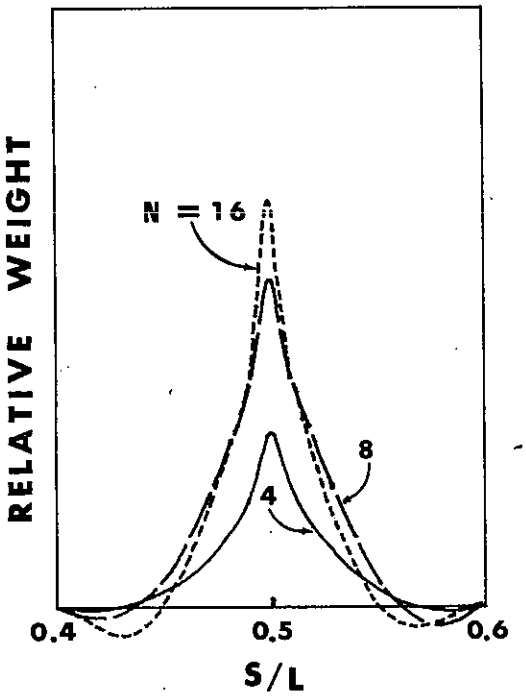

Figure 4. Path-weighting functions for crossed-path spatially filtered detector-array technique for C_n^2 measurements, where $\rho_0=\rho_t=4(\lambda L)^{\frac{1}{2}}$, d=0.2 and N is the number of detectors per array.

The results of the path-weighting functions for wind measurements (23) are shown in figure 5 with $\rho_0=\rho_0=4\sqrt{\lambda L}$ and the spatial wavelength d varying from 0.2 to 2(N=4). Again, the dash-line curve (d=2) is similar to the results obtained without using a spatially filtered receiver. When we decrease the spatial wavelength, the wind weighting functions become sharper with almost no side-lobes. Because the signal level is roughly proportional to the area under the weighting function, for smaller spatial wavelengths we have a weaker signal level that may not have enough SNR for the measurements. However, we can boost the signal by introducing more detectors per array. Figure 6 shows the results of having $\rho_0=\rho_t=4\sqrt{\lambda L}$, d=0.2 and varying the number of detectors N from 4 to 16. The shape of the weighting functions is about the same; the area under the curve is roughly proportional to the number of detectors. In case of necessity, of course, we can use more

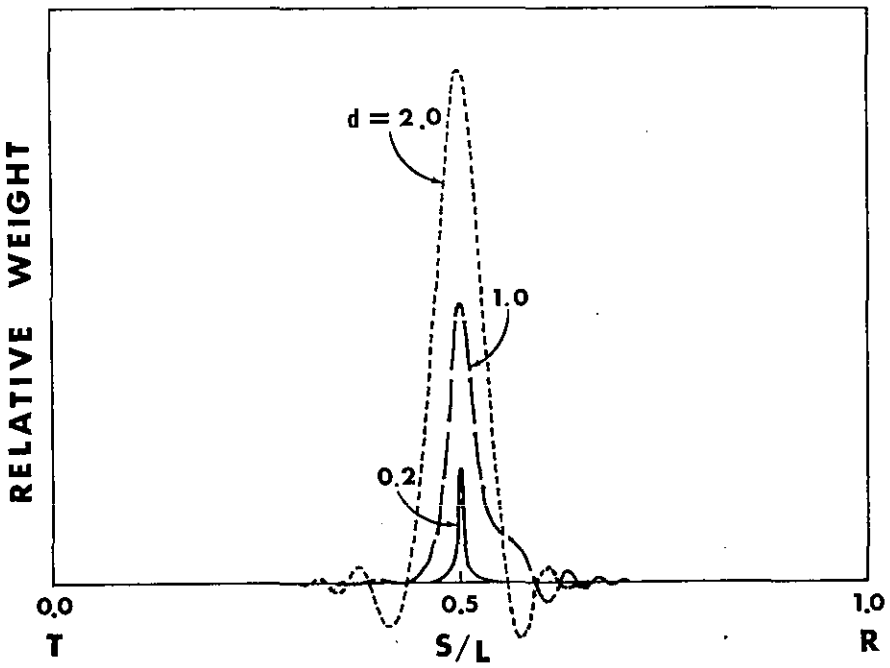

Figure 5. Path-weighting functions for crossed-path spatially filtered detector-array technique for wind measurements, where $\rho_0=\rho_t=4(\lambda L)^{\frac{1}{2}}$, *N=4 and d is the spatial wavelength.*

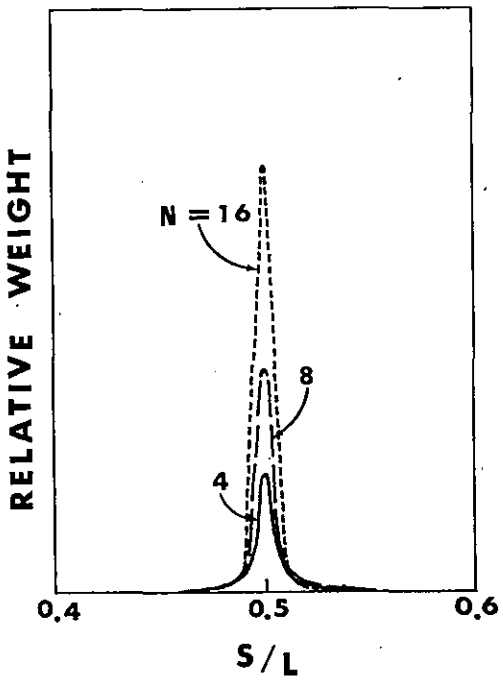

Figure 6. Path-weighting functions for crossed-path spatially filtered detector-array technique for wind measurements, where $\rho_0=\rho_t=4(\lambda L)^{\frac{1}{2}}$, *d=0.2 and N is the number of detectors per array.*

detectors to have an even stronger signal. Since the spatial wavelength is so small, the physical size of the array is not a problem. Note also that the width of the weighting function shown in figure 6 is only 2% of the total path.

It is surprising how different the changes are between the path-weighting functions for C_n^2 measurements and for wind measurements for small spatial wavelengths, while they are essentially the same for large spatial wavelengths. The physical explanation is as follows. Since we take the derivative of the time-lagged covariance function at zero-delay for wind measurements, we emphasize the contribution from smaller eddies for wind measurement more than for the C_n^2 measurement. When we use an imperfect spatial filter (which is true for a plus and minus alternately weighted array), the contribution from larger eddies is more important for C_n^2 measurments than for wind measurements. Hence, for the same spatial wavelength ($d \leq l$), the C_n^2 weighting function is broader than the wind weighting function (see Figs. 4 and 6).

The results for unresolvable sources are similar to those for resolvable sources (Figs. 3-6); hence we will not repeat them here.

3. EXPERIMENTAL TESTS

3.1 Resolvable Array

The theory presented in section 2.1 indicates that a crossed-beam system using coded light sources and 4-element array receivers is capable of effectively profiling wind and C_n^2. We have shown that the principle is sound by an experiment conducted on our 500-m test range on Table Mountain. Polarization-coded lasers and 4-element array receivers were used in the geometry shown in figure 1. The slope of the covariance of the quadrature array signals was compared with the reading of the anemometer at the cross-over location. A weighting function was also determined by using 6 anemometers clustered around the expected peak response. Plots of the optical measurement vs. the anemometer and of the weighting function measurement are shown in figure 7. Since the slope contains both wind and C_n^2 information, the measurement is more noisy (that is it has more scatter in the experimental points) than is expected when the complete proposed system is used. It does, however, illustrate the validity of this technique for path profiling.

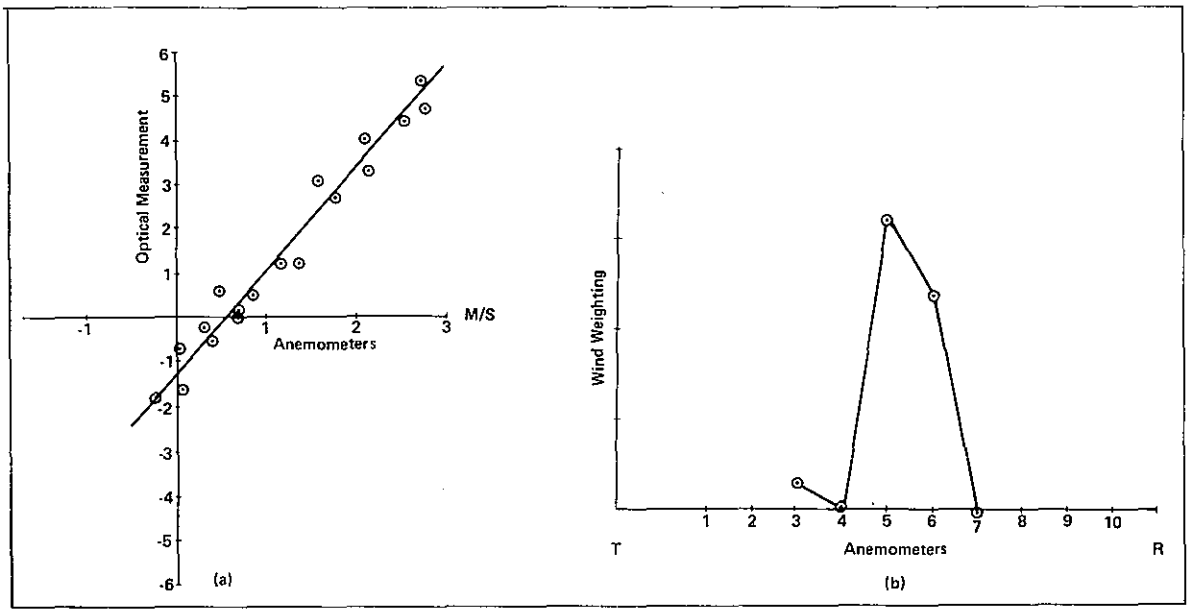

Figure 7. Experimental results for crossed-path spatially filtered detector-array technique for wind measurement. (a) Optical measurement vs. anemometer measurements (b) Path-weighting function.

We have also run tests with the arrays in phase (no horizontal displacement). The time-averaged product was proportional to the average C_n^2 value over the path but we have not yet made weighting function measurements for C_n^2 profiling with 4-element receiving arrays. However, previous work (Ochs et al., 1974) with 2-element arrays has shown experimentally that the principle is sound.

3.2 Unresolvable Array

Measurements to date, using two unresolved sources and three receivers for wind profiling, have not revealed the degree of sharpness indicated by the theory. The results are shown in figure 8. Circled points are experimental weighting function measurements where the outputs from ten anemometers measuring the crosspath wind component have been averaged in pairs and compared with the optical measurement. The crosses are the weighting results obtained by comparing the optical result with results from individual anemometers at the path locations indicated. While the response peaked at the appropriate location, the function was broader than expected. The reasons for this discrepancy are not fully understood.

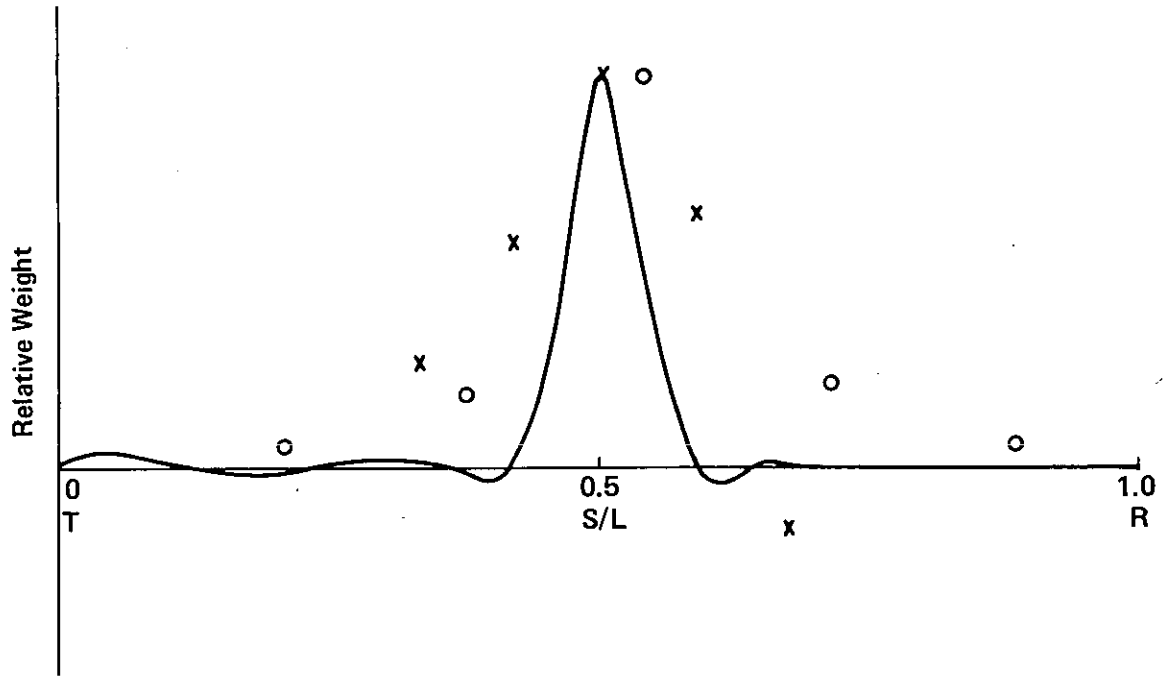

Figure 8. Theoretical (solid line) and experimental results of wind measurement, where $\rho_\ell = \rho_t = 3(\lambda L)^{\frac{1}{2}}$ *and N=1 (see Fig. 2c). Circled points are measurements that have been averaged in pairs; crosses are measurements of five center anemometers.*

4. PROPOSED PROFILING SYSTEMS

We plan to design a system that will path-resolve wind and C_n^2 into six parts over the middle two-thirds of an optical path. Three systems are under consideration. All, however, utilize the basic scheme of crossing light paths in a plane perpendicular to the component of the wind being measured. The basic crossover geometry for the first system is shown in figure 9. Two lasers (T1 and T2), polarization coded and separated vertically, radiate spherical waves to receivers R11 through R16 and R21 through R26, respectively. Receiver arrays R11 and R21 measure at position 1, R12 and R22 at position 2, and so on to position 6. The receiver detector configuration is shown in figure 10. The spatial wavelength of each array pair decreases from the crossover 1 to the crossover 6 pair to maintain an approximately uniform weighting function for each crossover. If the wavelength is not changed, the weighting function at the crossover increases greatly from crossover 1 to crossover 6 because of the large decrease in the angle of intersection. By increasing the wavelength, we counteract the

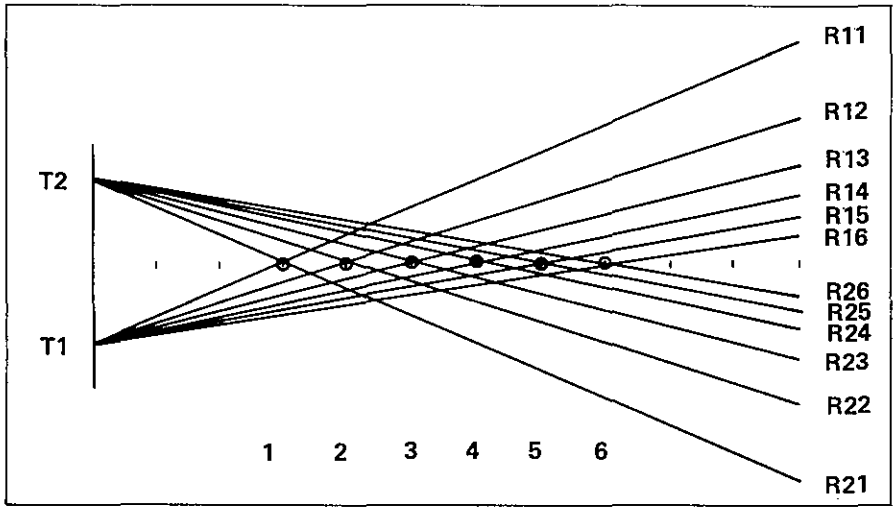

Figure 9. Horizontal view of cross-path geometry. The vertical scale is greatly exaggerated.

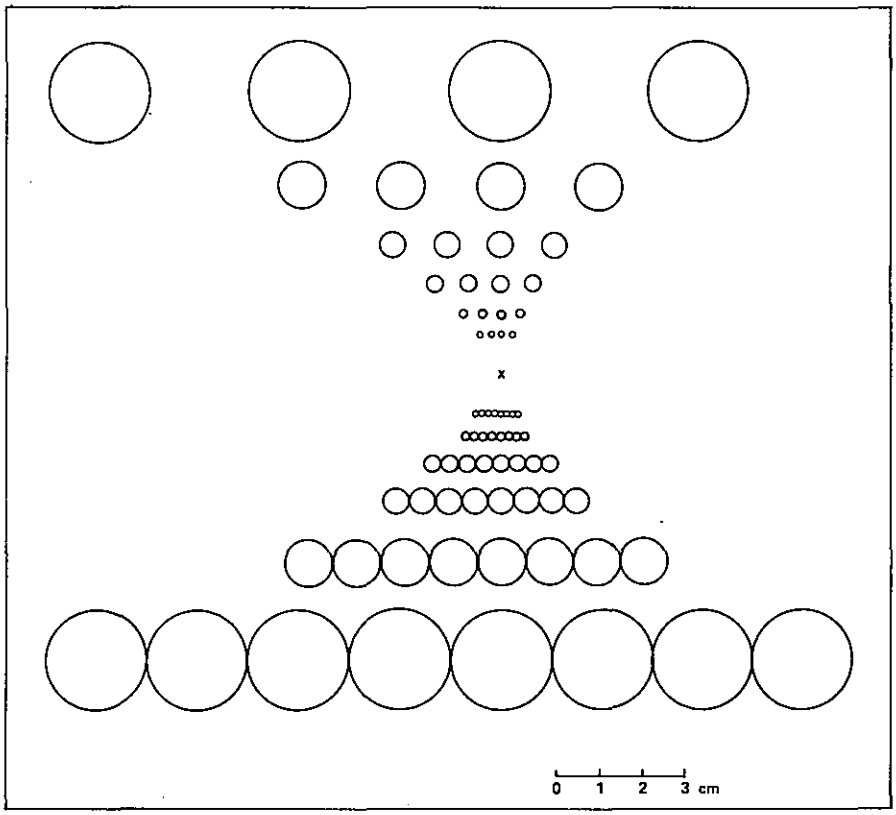

Figure 10. Detector configuration to measure six path locations simultaneously.

effect of changing the crossover angle. It may be necessary to compromise this adjustment and settle for weighting functions of different length in order to obtain sufficient signal strength for crossovers 5 and 6. In addition to the signal strength problem, the minimum useable spatial wavelength must be at least twice the inner scale of turbulence. If it were not for these restrictions, smaller spatial wavelengths could be used to advantage as the resultant weighting functions have very small sidelobes. In table I we list the detector spacings chosen for path lengths 0.5 to 2 km and ρ_t=2.52 cm.

Table I. Detector spacings

Position on path	ρ_0	d
1	13.4 cm	9.34 cm
2	8.82	4.60
3	6.05	2.52
4	4.20	1.46
5	2.88	0.86
6	1.89	0.50

The processing electronic logic is shown in figure 11 for one crossover pair. To maintain zero mean spatial filters, and also to maintain C_n^2 calibration independent of signal strength, we take the difference of the logarithms of alternate detectors in each array. The product of the in-phase spatially filtered signals is proportional to C_n^2 in the crossover volume defined by the weighting functions derived earlier. Logarithmic amplifiers may be used in this fashion for C_n^2 measurement when the refractive turbulence over the whole light path is small. It may be necessary to alter the system somewhat for the high refractive-turbulence case.

The pair of spatial arrays in phase quadrature is used for the wind measurement. We are developing a real-time processor that will examine the time covariance of the signals and determine what time scale a model covariance function should have to best fit the observed covariance. Since the spatial wavelength at the beam crossover is known, the wind speed is determined by this measurement.

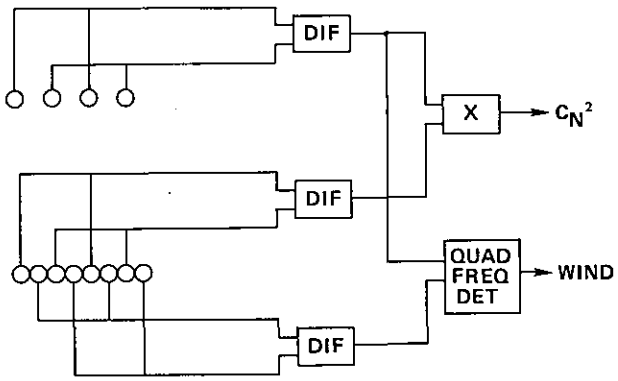

Figure 11. Block diagram of processing electronics for one of the six path locations to be measured.

An alternate optical system for path profiling is shown in figure 12. Beam expanders convert the lasers to plane wave sources large enough to illuminate detector arrays R1 and R21 through R26. The obvious advantage of this arrangement is to simplify the receiving system significantly. Only 32 detectors are required and only 8 log difference calculations rather than 18 are required, considerably simplifying the electronics. Disadvantages include the more complicated and expensive transmission optics and the fact that vertical beam bending due to regular refraction will make it difficult to keep the lasers pointed at the receiver system for near-ground light paths.

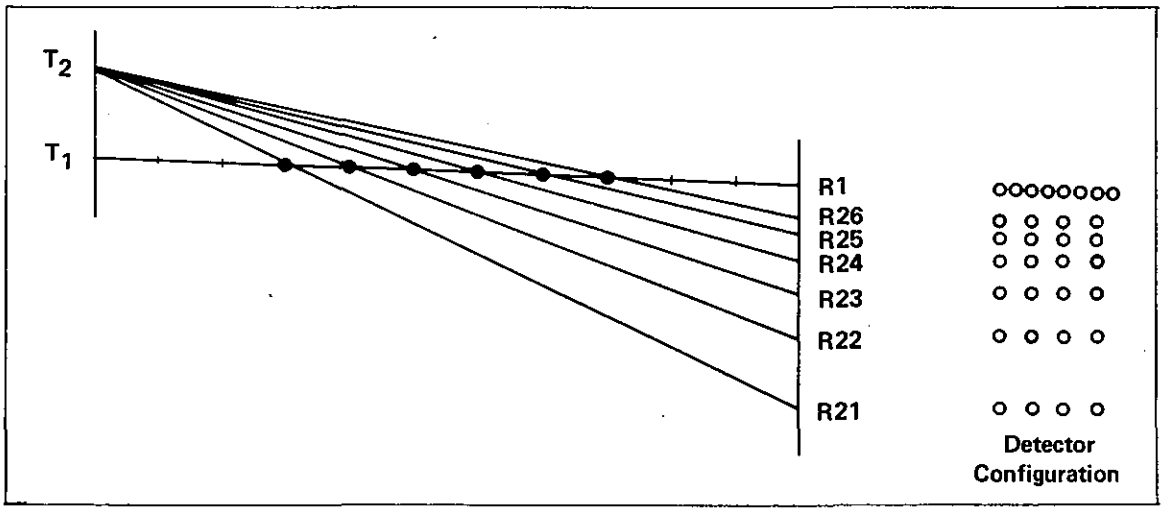

Figure 12. Horizontal view of cross-path geometry of a plane wave system.

Another possibility is to use coherent horizontal line sources, with sufficient vertical beam spread to cover the vertical beam bending. The geometry is shown in figure 13, with T1 and T2 coherent horizontal line sources. Only 32 elements are required in the receiving arrays, and correspondingly less complex electronics. The arrays must be unequally spaced in the vertical direction, however, and again the light sources are more complex.

5. DISCUSSION

All three proposed systems are under active consideration; more field experiments are required to determine which one will best satisfy the profiling requirements. Some additional theoretical development will be required if either of the plane wave systems are finally adopted.

We have shown that the slope of the normalized covariance is proportional to the crosspath windspeed at the geometric crossover point of two light paths to the receiving arrays. The slope of the function is also sensitive to variations of C_n^2 in the crossover volume. While it is possible to correct for this effect, it appears that a system that determines wind speed by observing the time scale (abscissa) of the covariance function will have better signal-to-noise. We have previously used the slope of the function to determine wind speed where an average over a path was desired, and have pointed out that frequency methods such as that proposed above for wind measurement do not average properly. However, if the measurement takes place over a small enough portion of the path, variations in wind speed within the volume are relatively small and such problems as winds crossing the path from two directions at once are unlikely. Thus true averaging is not a critical need and a frequency method may be used.

The C_n^2 measurement will be more difficult to make because in high turbulence there will be some change in the calibration due to saturation effects. We are not certain how serious these effects will be.

6. REFERENCES

Clifford, S. F. (1971); Temporal-frequency spectra for a spherical wave propagating through atmospheric turbulence. *J. Opt. Soc. Am.* 61:1285-1292.

Lawrence, R. S., G. R. Ochs, and S. F. Clifford (1972): Use of scintillation to measure average wind across a light beam. *Appl. Opt.* 11:239-243.

Lee, R. W., and J. C. Harp (1969): Weak scattering in random media, with applications to remote probing. *Proc. of IEEE* 57:375-406.

Ochs, G. R., S. F. Clifford, R. S. Lawrence, and Ting-i Wang (1974): Development of a ground-based optical method for measuring atmospheric turbulence aloft, NOAA Tech. Rept. ERL 297-WPL 30.

Ochs, G. R., G. R. Miller, and E. J. Goldenstein (1976a): A saturation-resistant system for measuring average wind, NOAA Tech. Memo. ERL WPL-14.

Ochs, G. R., S. F. Clifford, and Ting-i Wang (1976b): Laser wind sensing: the effects of saturation of scintillation. *Appl. Opt.* 15:403-408.

Tatarskii, V. I. (1961): *Wave Propagation in a Turbulent Medium*, translated by R. S. Silverman, McGraw-Hill Book Co., Inc. New York, N. Y. 285 pp.

Tatarskii, V. I. (1971): *The Effects of Turbulent Atmosphere on Wave Propagation*, National Technical Information Service, Springfield, Va., 472 pp.

Wang, Ting-i, S. F. Clifford, and G. R. Ochs (1974): Wind and refractive-turbulence sensing using crossed laser beams. *Appl. Opt.* 13:2602-2608.

☆GPO 1976 — 677-347/1272 REGION NO. 8